All-sky polarization imaging of cloud thermodynamic phase

LAURA M. ESHELMAN, MARTIN JAN TAUC, AND JOSEPH A. SHAW*

Department of Electrical and Computer Engineering, 610 Cobleigh Hall, Montana State University, Bozeman, Montana 59717, USA *joseph.shaw@montana.edu

Abstract: Knowing the cloud thermodynamic phase (if a cloud is composed of ice crystals or liquid droplets) is crucial for many cloud remote sensing measurements. Further, this knowledge can help in simulating and interpreting cloud radiation measurements to better understand the role of clouds in climate, weather, and optical propagation. Knobelspiesse et al. [Atmos. Meas. Tech. **8**, 1537, (2015)] showed that, for simulated zenith observations, the algebraic sign of the S₁ Stokes parameter (related to the difference between perpendicular and parallel linear polarization in the scattering plane) can be used to detect cloud thermodynamic phase when observed with a ground-based passive polarimeter. In this paper, we describe the use of our all-sky imaging polarimeter to experimentally test this proposed method of detecting cloud thermodynamic phase in the entire sky dome. The zenith cloud phase was validated with a dual-polarization lidar instrument.

© 2019 Optical Society of America under the terms of the OSA Open Access Publishing Agreement

1. Introduction

Clouds cover approximately 60 percent of Earth's surface and they play a significant role in the climate system, as they can regulate surface precipitation, shade the Earth's surface, and increase the greenhouse effect; however, they are one of the biggest sources of uncertainty in models [1–3]. Clouds also strongly attenuate optical propagation through absorption and scattering [4–9]. The absorption and scattering of clouds, and their net warming or cooling effect, depends on their physical properties, such as height, optical thickness, size, shape, and thermodynamic phase (if they contain ice crystals or liquid particles). Retrievals of cloud properties from satellite, airborne, and ground-based measurements also require cloud phase to be determined [10–12].

Cloud thermodynamic phase has been measured previously using both active and passive instruments. Active cloud lidar [13–16] and radar systems [17,18] with polarization sensitivity can distinguish between ice and water clouds. For example, the polarization state of light scattered from polyhedral ice crystals is altered so that there is a significant fraction of cross-polarized light (i.e., light oriented perpendicular to the transmitted light polarization state), whereas light undergoing single scattering by liquid water droplets retains its transmitted polarization state (i.e., the cross-polarized signal is effectively zero).

Cloud phase also can be retrieved from passive measurements of radiance emitted or scattered by clouds. These methods use one or more channel with absorption that is higher for ice than for liquid and one channel with nearly equal absorption for both ice and liquid. For example, this has been done with thermal infrared channels at 8.5, 11, and 12 μ m [19], 3.7, 11, and 12 μ m [20], and with a continuous spectrum between 11 and 19 μ m [21]. Another method added a visible channel at 0.65 μ m and short-wave infrared (SWIR) channels at 1.63 and 1.90 μ m along with thermal IR channels at 8.5, 11, and 12 μ m [22]. SWIR methods have been demonstrated using channels at 1.64 and 1.70 μ m [23–25] and 1.55, 1.64, and 1.70 μ m [26], while a near-infrared method relied on spectra in the wavelength range of 850-1050 nm, in which ice absorption was found to be higher than water absorption for certain parts and lower in other parts [27].

Recently, Knobelspiesse et al. [28] showed that the direction of linear polarization (expressed by the sign of the Stokes S_1 parameter defined in the solar scattering plane) should be useful for determining cloud thermodynamic phase with a passive ground-based polarimeter. The solar scattering plane contains the directions of incident sunlight and scattered light. A positive S_1 value indicates a liquid cloud with linear polarization parallel to the scattering plane, while a negative S_1 value indicates an ice cloud with linear polarization perpendicular to the scattering plane. They provided initial validation of simulation results using zenith-pointing, polarization-sensitive Cimel radiometers from the NASA Aerosol Robotic Network (AERONET).

The objective of our study was to detect cloud thermodynamic phase using a ground-based, all-sky imaging polarimeter following the same method. The Knobelspiesse et al. simulations suggested that the optimal measurement for cloud thermodynamic phase was not at the zenith, but in a direction in the solar principal plane approximately 55° from the sun. With our calibrated all-sky polarimeter operating in 10-nm-wide wavelength bands centered at 450 nm, 490 nm, 530 nm, 670 nm, and 780 nm, we were able to verify this. We detected ice, liquid, and multi-layered ice and liquid clouds using the measured S₁ Stokes parameter and we independently verified our results using dual-polarization lidar measurements at the zenith. In the balance of this paper, Section 2 provides a description of our methodology, Section 3 shows our measurements and results, Section 4 offers a discussion, and Section 5 outlines our conclusions.

2. Methodology

In this paper, we demonstrate that an all-sky imaging Stokes polarimeter can be used to detect cloud thermodynamic phase by analyzing the Stokes S_1 parameter, measured relative to the scattering plane. Simulations from Knobelspiesse et al. [28] showed that the direction of linear polarization (as expressed by the sign of the Stokes S_1 parameter defined in the solar scattering plane) is an indication of cloud thermodynamic phase. Positive or slightly negative values of S_1 indicate a liquid cloud with linear polarization parallel to the scattering plane, while more negative values of S_1 indicate an ice cloud with linear polarization perpendicular to the scattering plane. Since we used all-sky polarization images from a multi-month campaign and did not focus solely on principal-plane measurements, we found similarities and differences from what was described in their paper. These are discussed further in Sections 3 and 4.

2.1 All-sky imaging polarimeter overview

To detect cloud thermodynamic phase, we used a ground-based, all-sky imaging polarimeter operating at visible and near-infrared wavelengths. This instrument was developed at Montana State University and uses a fisheye lens to image the sky with a field of view of approximately 160° [29]. We have used this polarimeter to study skylight degree of linear polarization (DoLP) and angle of polarization (AoP) for clear and partly cloudy skies [30,31] and have performed careful comparisons of clear-sky measurements with a polarized radiative transfer model [32], which was then used to explore the spectral variation of skylight polarization across the visible-NIR-SWIR spectrum [33,34]. For the present study, the instrument operated in 10-nm-wide wavelength bands centered at 450 nm, 490 nm, 530 nm, 670 nm, and 780 nm. In this imager, two liquid crystal variable retarders (LCVRs) were used to electronically vary the retardance seen by incoming light so that a full Stokes image was measured in less than a few tenths of a second at each wavelength. The LCVRs allowed rapid acquisition that enabled reliable measurement in partly cloudy skies by avoiding polarization artifacts from inter-frame cloud motion. The polarimeter was calibrated using an external rotating polarizer and an integrating sphere viewed at numerous angles to fully capture the imager's system matrix over the entire fisheye field of view. Maximum error for the Stokes S_1 and S_2 parameters was estimated as $\pm 1.2\%$ with 100% linear input [29].

2.2 Dual-polarization lidar overview

A dual-polarization lidar [14] was used to validate zenith cloud thermodynamic phase measurements taken with the all-sky polarimeter. This lidar uses a liquid crystal variable retarder in the receiver to alternate between co-polarized and cross-polarized polarization states of the backscattered signal from alternate laser pulses at a rate of 30 pulses/s. The laser source is linearly polarized and the two received signals are either parallel (co-polarized) or orthogonal (cross-polarized) to the laser signal. The cross-polarization ratio (δ) was measured as a ratio of the cross-polarized and co-polarized signals. This ratio identifies the presence of ice crystals in the clouds since light scattered from polyhedral ice crystals has a significant fraction of cross-polarized light, while light singly scattered from water droplets does not. The physical basis, capabilities, and uncertainties of this classic method are discussed in [13].

3. Measurements and results

The all-sky polarimeter and dual-polarization lidar were operated together at times when ice, liquid, and multi-layered clouds were present throughout a multi-month period in Bozeman, Montana, USA (latitude: 45.6667; longitude: -111.0451). Example images showing S_0 , S_1 , DoLP, and AoP measured at 530 nm are displayed in Fig. 1. These examples include an ice cloud from 25 October 2016, a liquid cloud from 28 August 2018, multi-layered clouds from 5 July 2016, and clear sky from 15 February 2017. The solar zenith angles for these measurements were 65.9° , 41.4° , 23.1° , and 58.4° , respectively. The images are shown with the top of the image representing north and the right side of the image representing west, and with angles measured relative to the scattering plane.

Stokes S_0 and DoLP images were used to determine the presence of clouds. Cloudy pixels were identified by higher radiance values in the S₀ images or lower values in the DoLP images relative to the background sky because of multiple scattering within the cloud [31,35]. However, because the AoP for ice clouds is aligned perpendicular to the scattering plane, the same as the clear sky, polarization angle alone is not a reliable indicator of clouds or cloud phase. The S₁ images, however, look significantly different for the different cloud types. Most importantly, in agreement with the theoretical predictions, the ice cloud in Fig. 1 produced negative S_1 values (average value = -0.056), while the liquid cloud produced positive values (average value = 0.003). The multi-layered cloud in Fig. 1 showed positive S_1 values for the liquid clouds and negative S₁ values for the ice clouds seen through the gaps in the liquid clouds (average ice value = -0.016; average liquid value = 0.001). In this figure, the ice clouds are identified by the negative S₁ values (corresponding to an AoP perpendicular to the scattering plane), while the liquid clouds are identified by the positive S₁ values (corresponding to an AoP parallel to the scattering plane). The background skylight in all cases was polarized perpendicular to the scattering plane. In the examples presented, notice that cloud phase can be observed in the entire image, not just at the zenith.

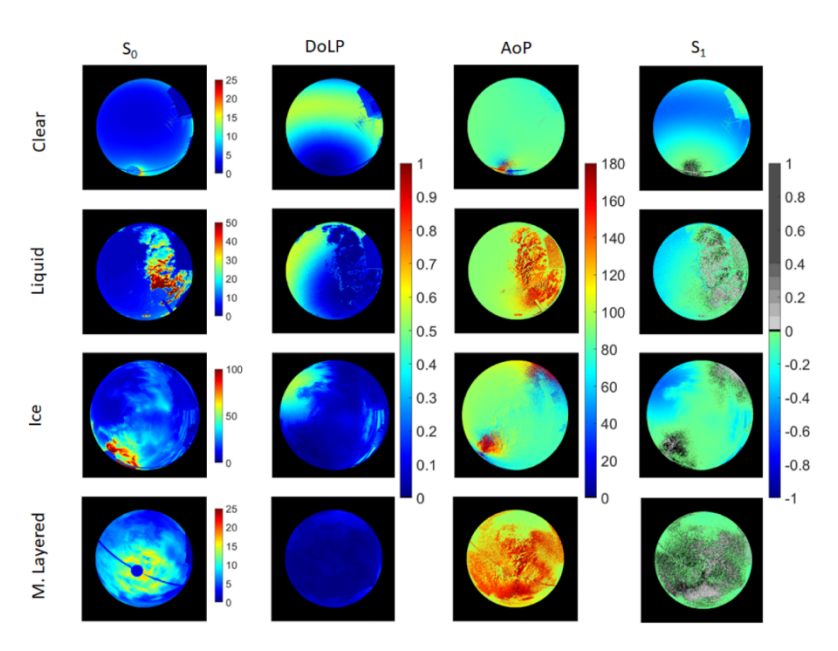


Fig. 1. All-sky polarimeter S_0 , S_1 , DoLP and AoP images referenced to the scattering plane. The measured S_1 values for the entire sky-dome indicate the presence of ice clouds on 25 October 2016, a liquid cloud on 28 August 2018, and multi-layered (ice and liquid) clouds on 5 July 2016. Negative values of S_1 indicate ice and positive values of S_1 indicate liquid cloud phase. A clear-sky on 15 February 2017 is representative of a Rayleigh atmosphere where positive values of S_1 indicate linear polarization parallel to the scattering plane and negative values of S_1 indicate linear polarization perpendicular to the scattering plane. For the all-sky images, the top of the image represents north and the right side of the image represents west.

3.1 Zenith measurements

A summary of 27 different zenith measurements at each all-sky polarimeter wavelength, validated with the dual-polarization lidar, are shown in Fig. 2, with corresponding data listed in Table 1. The listed S₁ parameters were calculated by masking a region of clouds near the zenith (in a cone of 5° radius) and by averaging the masked S₁ values for the cloud pixels. A mask of the cloud pixels was created by normalizing the S_0 image and selecting values greater than the background skylight. In Table 1, the zenith angles correspond to the scattering angles in the solar principal plane, similar to the simulations presented in Knobelspiesse et al. [28] (the scattering angle is defined as the angle between the solar illumination direction and the scattered direction). The zenith angles in parentheses correspond to cloud pixels measured off-axis (i.e. not at the zenith) with the same cloud-identification procedure applied. A positive or slightly negative S₁ value theoretically indicates a liquid cloud, while a more negative value indicates an ice cloud. Accordingly, we measured negative S₁ values for ice clouds (verified at the zenith with the lidar) and both negative and positive values for verified liquid clouds. We detected cloud phase for multiple days with solar zenith angles ranging from 23° to 72°. Lidar validation measurements are presented in Fig. 3. A lidar crosspolarization ratio less than 0.08 indicates liquid, while a cross-polarization ratio greater than 0.08 indicates ice (the cross-polarization ratio for liquid phase should be approximately zero; however, multiple scattering can lead to cross-polarization ratios above zero). Notice that in Fig. 3 there is a clear separation between the verified liquid and ice S_1 values.

Table 1. All-sky polarimeter (S_1), dual-polarization lidar, and AERONET data. For each day, the time of measurement (UTC) as well as the solar zenith (Ze) angles were recorded (time notation: MMDD). Scattering angles in the principal plane (i.e. zenith measurement) correspond to the solar zenith angles. Angles in parentheses represent the zenith angle of cloud pixels measured off-axis. For each wavelength, the mean cloud phase retrieved from the polarimeter's Stokes S_1 image was recorded. Cloud phase measurements were validated using a dual-polarization lidar. The cross-polarization ratio (δ) indicates liquid (δ < 0.08) or ice (δ > 0.08) phase. The AERONET aerosol optical depth (AOD) corresponds to level 1.0 processed data at 500 nm. Missing values in the polarimetric measurements represent a time when the corresponding wavelengths were not measured. The measurement site latitude and longitude coordinates were 45.6667 and -111.0451, respectively.

1 2	Date 0123 0304	Diar Geom Time 2101	Ze	450 nm	490 nm	larimeter (S	670 nm	780 nm	Lidar	AERONET				
1 2	0123 0304		-	430 IIII	470 IIII			/XII nm	δ	AOD				
2	0304	2101					070 11111	700 1111	U	ПОБ				
2	0304	2101		2016										
			68	-0.202					0.47	0.20				
2	0204	1953	52	-0.156	-0.143	-0.119	-0.075	-0.053	0.40	0.19				
3 '	0304	2024	53	-0.139	-0.132	-0.104	-0.058	-0.038	0.40	0.08				
4	0401	2056	45	-0.008	0.003	0.010	0.023	0.025	0.03	0.03				
5	0401	2115	47	-0.027	-0.016	-0.006	0.016	0.021	0.02	0.07				
6	0401	2150	51 (46)	0.003	0.007	0.014	0.025	0.023	0.02	0.07				
7	0401	2234	57 (50)	-0.040	-0.026	-0.014	-0.004	-0.003	0.02	0.02				
8	0630	1811	27	-0.002	-0.001	0.001	0.002	0.005	0.03	0.36				
9	0705	1941	23	-0.011	-0.014	-0.016	-0.017	-0.009	0.39	0.66				
10	0705	1941	23	0.001	0.004	0.001	0.004	0.006	0.02	0.66				
11	0706	2016	25	0.000	-0.001	-7.2e-5	-0.003	-0.005	0.06	0.07				
12	0902	1838	39 (73)	-0.067	-0.041	-0.034	-0.005	0.009	0.03	0.21				
13	1018	2158	67	-0.125	-0.062	-0.049	-0.039	-0.025	0.40	0.01				
14	1021	1607	70	-0.096	-0.077	-0.064	-0.027	-0.016	0.03	0.36				
15	1025	1649	66	-0.086	-0.065	-0.056	-0.033	-0.017	0.41	0.04				
16	1107	1629	72	-0.227	-0.209	-0.181	-0.107	-0.071	0.34	0.17				
2018														
17	0731	1455	63	-0.078	-0.074	-0.072	-0.078	-0.075	0.31	0.16				
18	0803	1721	39 (73)	-0.112	-0.115	-0.127	-0.180	-0.203	0.11	0.47				
19	0816	1525	59	-0.178	-0.174	-0.173	-0.193	-0.191	0.18	0.24				
20	0822	2232	62	-0.062	-0.053	-0.034	-0.038	-0.033	0.04	0.47				
21	0828	2059	41 (24)	0.002	-0.001	0.003	0.005	0.006	0.05	0.08				
22	0830	2019	39	-0.004	-0.006	-0.005	-0.005	-0.011	0.03	0.20				
23	0919	1918	44	-0.065	-0.057	-0.049	-0.033	-0.034	0.04	0.27				
24	0920	1543	65	-0.003	-0.002	0.001	0.015	0.010	0.03	0.12				
25	0920	2307	67 (20)	-0.020	-0.020	-0.018	-0.013	-0.009	0.02	0.10				
26	0926	1735	52	-0.165	-0.137	-0.137	-0.075	-0.073	0.33	0.08				
27	0928	2012	50	-0.064	-0.050	-0.044	-0.022	-0.009	0.32	0.07				

In our observations shown in Fig. 2, clouds were generally more polarizing at shorter wavelengths for ice clouds and at longer wavelengths for liquid clouds, in agreement with the Knobelspiesse predictions. From Fig. 2, we determined a threshold of $S_1 = -0.04$ to distinguish between zenith-validated liquid and ice clouds. An S_1 value greater than -0.04 indicates liquid phase, while a S_1 value less than -0.04 indicates ice phase.

Polarimetric cloud phase determination was also observed to depend on scattering angle, especially for liquid clouds. The simulations of Knobelspiesse et al. [28] showed that ice clouds could be detectable between scattering angles of approximately 10^0 and 150° , while liquid clouds could only be reliably detected between scattering angles of 10^0 and 70° (using the baseline that ice clouds are negative and liquid clouds are positive). For liquid clouds, measured S_1 values were greatest between scattering angles of 10^0 and 60° , as observed in Fig. 4, which shows the S_1 scattering angle dependence with wavelength (for measurements validated at the zenith). Our optimal scattering angle was observed to be closer to 45° , not 55° as predicted by Knobelspiesse. For scattering angles greater than 60° , the classification of

liquid phase was observed to vary with wavelength. For clouds determined to be liquid with zenith lidar observations, S_1 measurements at 670 and 780 nm were greater than -0.04, while measurements at 450, 490, and 530 nm were less than -0.04. In general, ice clouds could be determined reliably for scattering angles from 0° to beyond 70° . The scattering angle dependence for the measured pixels in the entire field of view will be discussed further in section 3.2.

In Fig. 2, measurements 11, 18, and 19 were observed to have reverse wavelength dependence relative to the other measurements. Measurement 11 corresponds to verified liquid S_1 values, where measurements 18 and 19 correspond to verified ice S_1 values. These measurements were made on 6 July 2016, 3 August 2018, and 16 August 2018, respectively. The liquid S₁ values in measurement 11 could suggest a minimum scattering angle needed to reliably detect liquid phase based on spectral measurements. In this case, the scattering angle was 25° and S₁ values were greatest at shorter wavelengths. In measurements 18 and 19 (made at scattering angles of 73° and 59°, respectively), the aerosol optical depth at 500-nm wavelength was 0.47 and 0.24, respectively, indicating the atmosphere was quite smoky. It seems likely that this spectral reversal arose because the smoke layer was selectively depolarizing the shorter-wavelength light scattered from the cloud above; however, an alternate idea to consider is that the smoke aerosols could have enhanced the long-wavelength polarization, as we recently observed at SWIR wavelengths for thick wildfire smoke [35], although in those previous observations the smoke only enhanced the polarization for wavelengths longer than 1 μm . The S_1 dependence on aerosol optical depth can be observed in Fig. 5.

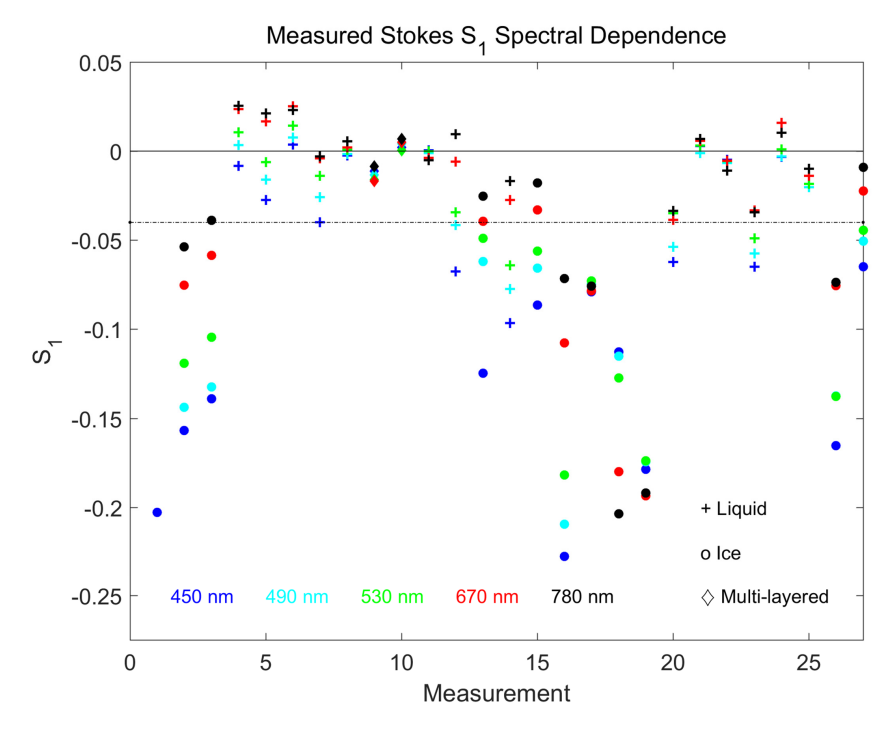


Fig. 2. Multi-wavelength all-sky polarimeter measurements validated with a dual-polarization lidar at the zenith. Liquid clouds are represented by the plus (+) symbols, ice clouds are represented by the unfilled circles (o), multi-phase clouds are represented by diamonds (◆). The 450, 490, 530, 670, and 780 nm measurements are represented by blue, cyan, green, red, and black colors, respectively. Ice clouds were generally found to have S₁ values less than −0.04 (dashed line) and liquid clouds tended to be both positive and negative at larger scattering angles.

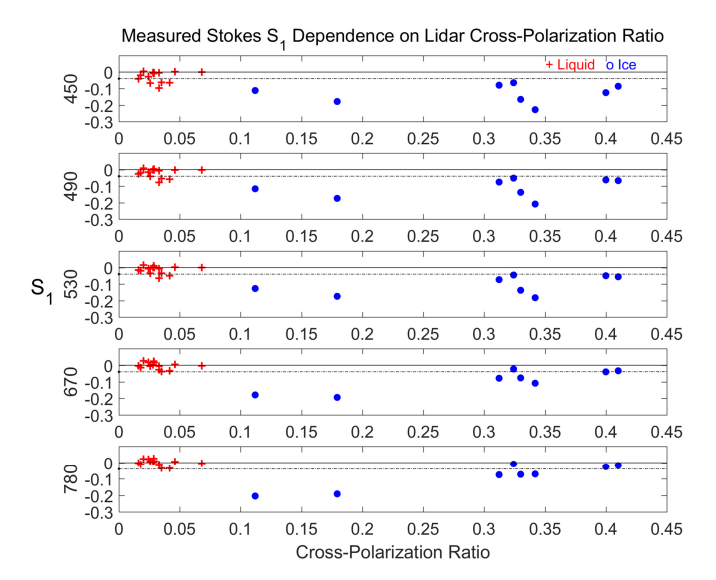


Fig. 3. The observed relationship between the Stokes S_1 parameter in the scattering plane and the lidar's measured cross-polarization ratio at the zenith for each wavelength. Liquid clouds are represented by the red plus (\pm) symbols, ice clouds are represented by the blue, filled circles (o).

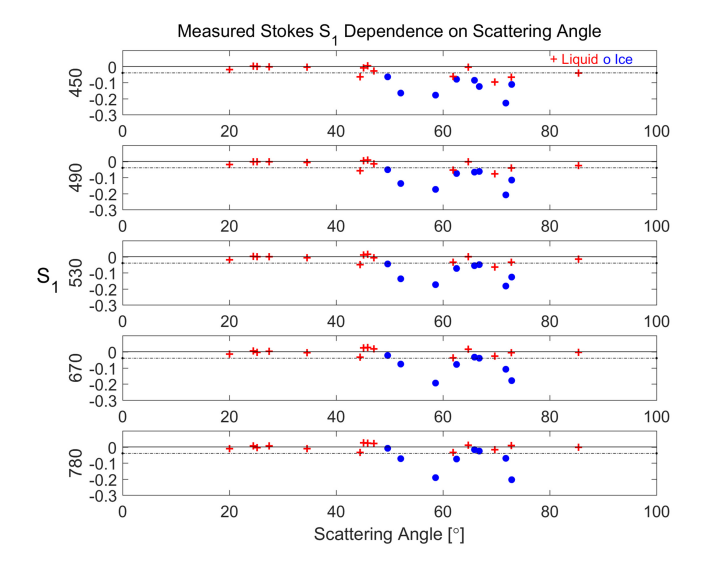


Fig. 4. The observed relationship between the Stokes S_1 parameter in the scattering plane at the zenith and the corresponding scattering angle for each wavelength.

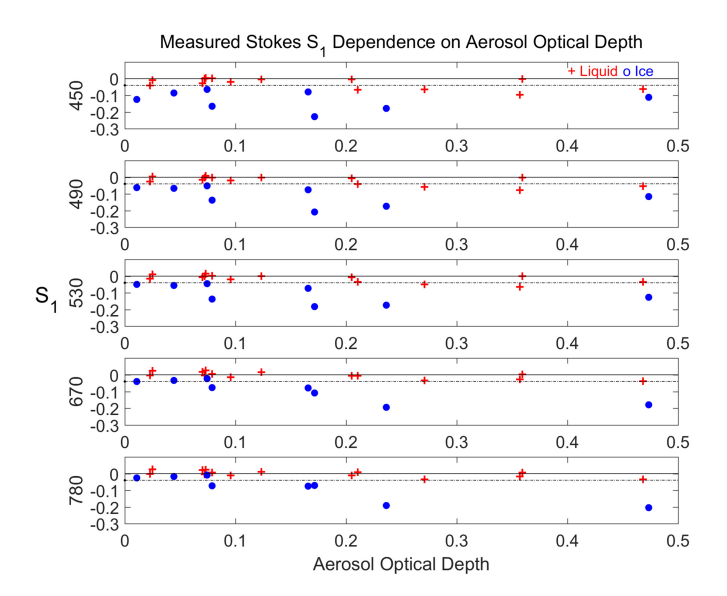


Fig. 5. The observed relationship between the Stokes S_1 parameter in the scattering plane and the AOD retrieved from AERONET for each wavelength. An observed switch in the spectral dependence was observed for ice clouds at AOD values greater than 0.2. Below an AOD value of 0.2, the S_1 value was greatest at shorter wavelengths. Above an AOD value of 0.2, the S_1 value was greatest at longer wavelengths.

3.2 All-sky measurements

In Fig. 6, all-sky images show the relationship between S_1 (referenced to the scattering plane) and scattering angle for the five polarimeter wavelengths in the entire sky-dome for a zenith-verified liquid example on 1 April 2016. This multi-wavelength example shows liquid clouds having greater S_1 values and more of the cloud being detected in the image at longer wavelengths. Scattering angles of 10^0 and 70° are shown on the images with black lines to indicate the approximate angular range in which liquid phase can be reliably identified. All-sky polarimeter S_1 images at 530 nm from 1 April 2016 and 31 July 2018 are also shown in Fig. 7 with scattering angles of 10^0 and 70° . Figures 6 and 7 show the significance of measuring cloud phase with respect to scattering angle when detecting liquid phase. Ice phase can be detected in the entire image of an all-sky Stokes S_1 image, where liquid phase detection is mainly bound between scattering angles of 10^0 and 70° and depends on wavelength.

A mask of the cloud pixels in Fig. 7 was created by normalizing the S_0 image and masking out values greater than the background skylight (if using a RGB camera system, cloud masking could be done using methods presented by [36]). We did not use a red/blue ratio to find clouds with the liquid-crystal-based all-sky imager because there is a multi-second delay between image sets at different wavelengths (this system provides rapid calculation of a polarimetric image sequence, but with a larger delay between spectral channels). The masked regions were then applied to the S_1 image, scattering angle image, and zenith angle image (Fig. 8) to visualize the measured S_1 dependence with scattering angle (Fig. 9) and zenith angle (Fig. 10) in the entire all-sky image. Ice clouds were generally found to have S_1 values less than -0.04 (dashed line), where liquid clouds tended to be both positive and slightly negative. At scattering and zenith angles greater than 60° and 25° , respectively, liquid clouds were found to have S_1 values less than -0.04.

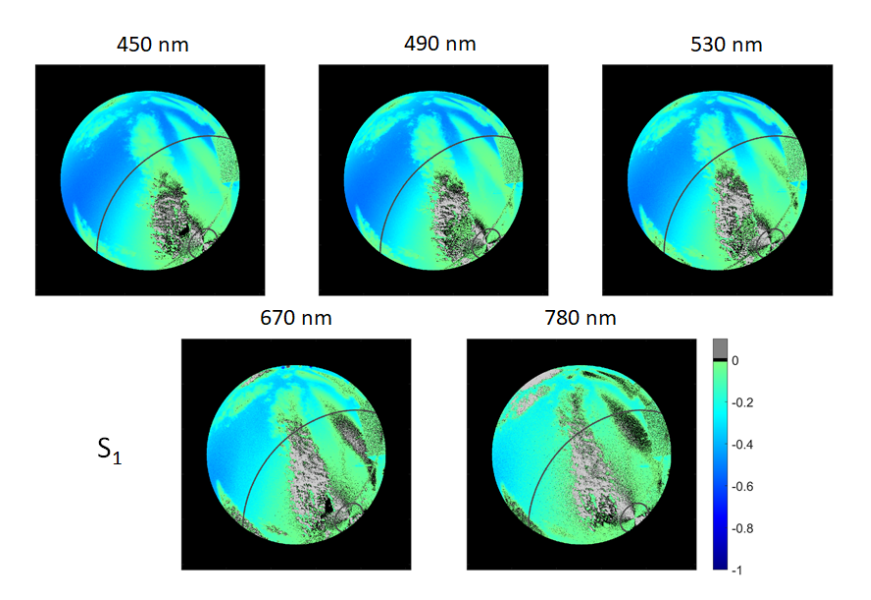


Fig. 6. The observed variation with wavelength of the Stokes S_1 parameter expressed relative to the scattering plane for a liquid cloud on 1 April 2016 for a solar zenith angle of 51° . Scattering angles of 10° and 70° are shown on the images with black lines.

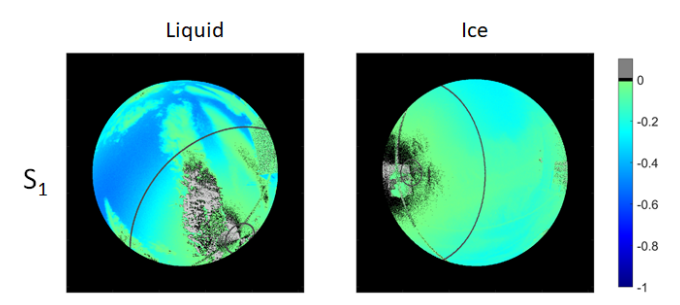


Fig. 7. All-sky polarimeter S_1 images at 530 nm from 1 April 2016 and 31 July 2018 showing liquid and ice clouds for solar zenith angles of 51° and 63°, respectively. Scattering angles of 10^0 and 70° are shown on the images with black lines.

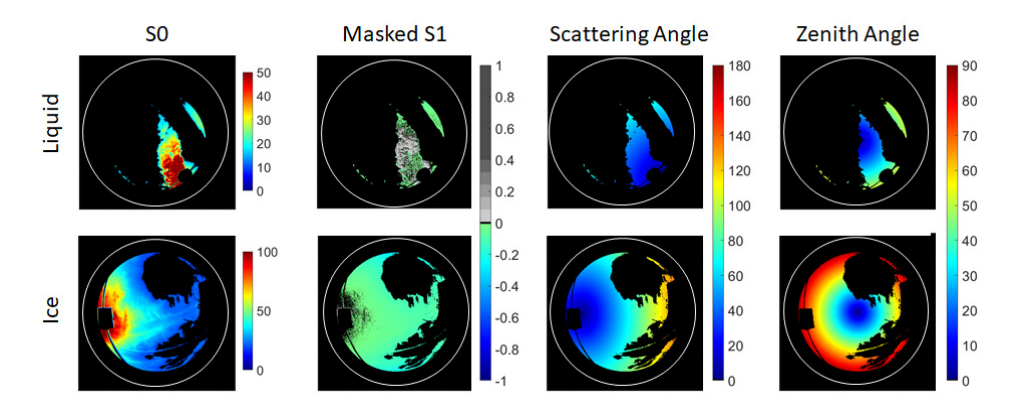


Fig. 8. Example of cloud pixel masking using the S_0 image to detect the presence of clouds, with corresponding masked cloud pixels in the S_1 , scattering angle, and zenith angle images.

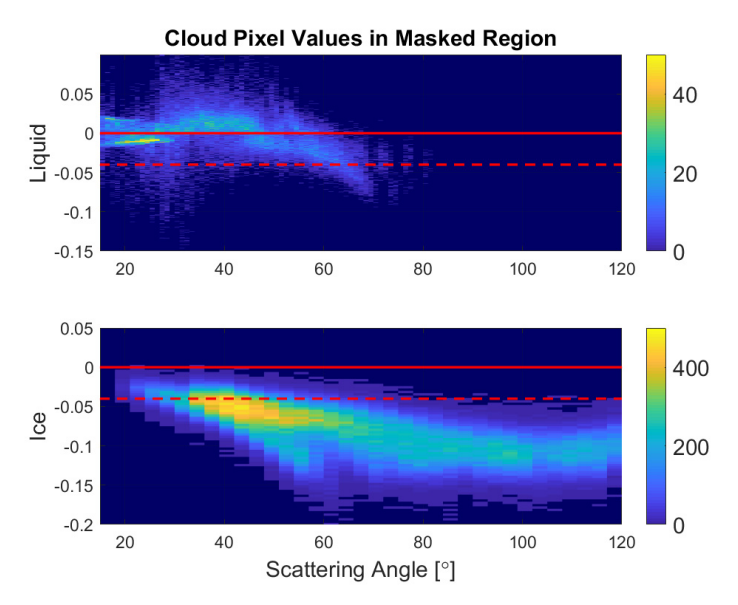


Fig. 9. The relationship between the measured cloud S_1 values (referenced to the scattering plane) and scattering angle for liquid clouds on 1 April 2016 (top) and ice clouds on 31 July 2018 (bottom) at 530 nm. Ice clouds were generally found to have S_1 values less than -0.04 (dashed line), where liquid clouds tended to be both positive and slightly negative. At scattering angles greater than 60° , liquid clouds were found to have S_1 values less than -0.04, thus overlapping with the range of S_1 values that would otherwise indicate ice clouds. The solar zenith angles were 51° and 63° , respectively.

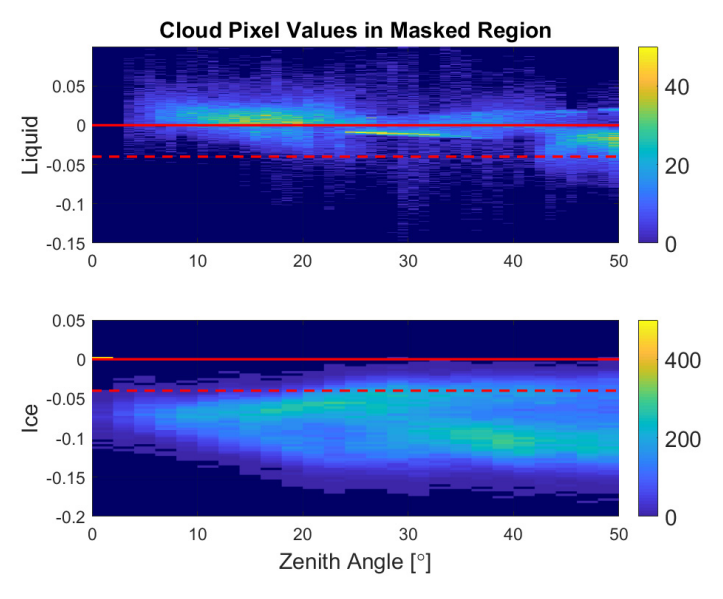


Fig. 10. The relationship between the measured cloud S_1 values (referenced to the scattering plane) and zenith angle for liquid clouds on 1 April 2016 (top) and ice clouds (bottom) on 31 July 2018 at 530 nm. Ice clouds were generally found to have S_1 values less than -0.04 (dashed line), where liquid clouds tended to be both positive and slightly negative. Liquid clouds tended to be more positive for zenith angles less than 25° . Ice clouds were negative for all zenith angles. The solar zenith angles were 51° and 63° , respectively.

4. Discussion

Careful observation guidelines must be considered when measuring cloud phase in the entire sky dome. First, the sun-cloud-observer geometry significantly affects the measured S_1 image. If the polarimeter's reference frame is not aligned to the scattering plane, the determination of cloud phase cannot be made accurately, as illustrated in Fig. 11. With S₁ expressed in the instrument's reference plane (IP), cloud phase is ambiguous and depends on the scattering geometry. However, expressing S₁ relative to the scattering plane (SP) for each pixel allows us to reliably detect liquid phase over the scattering angles of 10° to 70° (for Fig. 11, the lidar's cross-polarization ratio was approximately 0.02 at a cloud height of 3.5 km, indicating liquid-phase clouds). In other words, for a fisheye image it is necessary to rotate the polarimeter's frame of reference into the scattering plane reference [37] to determine cloud phase in the entire image, not just the principal plane. For measurements with a point-source polarimeter, the instrument could be deployed on an azimuthal mount so that the polarimeter's reference frame was always aligned with respect to the solar scattering plane (i.e. the reference polarizer would be parallel to the scattering plane). With the instrument aligned in this fashion, the polarimetric reference plane at each point would be the solar scattering plane unique to that position.

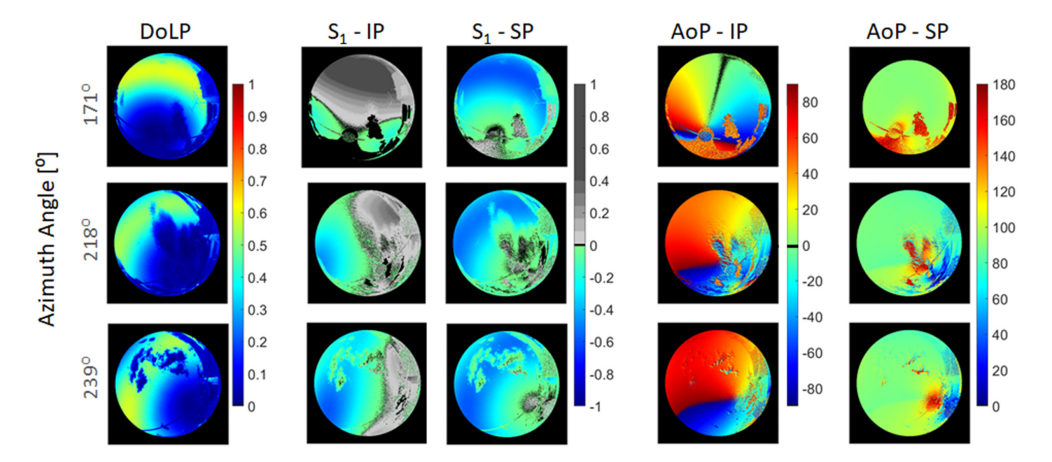


Fig. 11. DoLP, Stokes S₁, and AoP images in the instrument plane (IP) and scattering plane (SP) from 1 April 2016 with solar azimuth angles of 171°, 218°, and 239° and zenith angles of 41°, 47°, and 57°, respectively. This figure demonstrates the importance of aligning the polarimeter's reference frame to the scattering plane. In the polarimeter's reference frame, both phases are detected depending on the scattering geometry whereas in the scattering plane, liquid phase is detected over the scattering angles of 10° and 70° (the lidar's cross-polarization ratio was approximately 0.02 at a cloud height of 3.5 km (AGL), indicating liquid phase).

The spectral distribution of S_1 values in Fig. 2 suggests that it might be possible to use an RGB polarimeter [38] for fast spectral and polarimetric acquisition, possibly employing a red/blue ratio to identify clouds. Figure 12 shows that it may be possible to enhance the cloud phase identification by using two wavelengths, such as red and blue, because ice clouds tend to have larger S_1 magnitudes at shorter wavelengths (blue), where liquid clouds tend to have larger S_1 magnitudes at longer wavelengths (red). A common threshold of approximately -0.04 could be used or possibly separate thresholds could be found for the red and blue channels to identify cloud phase. However, these initial data suggest this classification may not always work for multi-layered clouds or for measurements at scattering angles greater than approximately 60° .

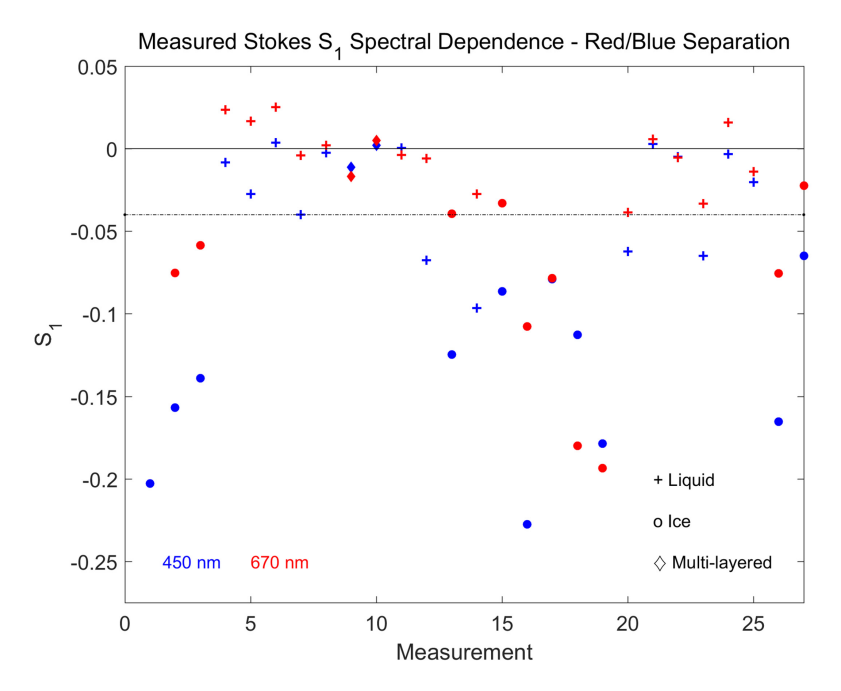


Fig. 12. Red/blue wavelength validated all-sky polarimeter measurements with a dual-polarization lidar at the zenith. Liquid clouds are represented by the plus (+) symbols, ice clouds are represented by the unfilled circles (o), multi-phase clouds are represented by diamonds (\bullet). The 450 and 670 nm measurements are represented by blue and red colors, respectively.

5. Conclusions

Following the method presented by Knobelspiesse et al. [28], we have detected cloud thermodynamic phase using the Stokes S₁ parameter at angles beyond the zenith. We used a zenith-pointed, dual-polarization lidar to validate the identification of ice, liquid, and multilayered clouds using the S₁ parameter rotated to be expressed relative to the scattering plane. Furthermore, we have experimentally shown the dependence of polarimetric cloud phase retrievals on the sun-observer scattering geometry. A positive or slightly negative S₁ value indicated a liquid cloud, while a more negative S₁ value indicated an ice cloud. Our data suggest an initial threshold of $S_1 = -0.04$. Compared to the study presented by Knobelspiesse et al., our measured S₁ parameters were found to be slightly greater than their simulated values in the scattering plane for ice clouds. For liquid clouds, we found S₁ values to increase in magnitude at longer wavelengths, and for ice clouds we found S₁ values to increase in magnitude at shorter wavelengths (matching the simulations presented by Knobelspiesse et al). S₁ values are strongly dependent on scattering angle and the optimal scattering angle to detect liquid clouds was approximately 45° in our data, compared to 55° in the Knobelspiesse et al. simulations. Among our five all-sky polarization imager spectral bands, the optimal wavelengths to detect cloud phase with a visible polarimeter were found to be red (670 nm) for liquid and blue (450 nm) for ice.

Our main objective was to verify that the ground-based all-sky polarimeter system reliably determined cloud thermodynamic phase, as validated at the zenith with a dual-polarization lidar. The results of this study strongly suggest this method could be used to determine cloud thermodynamic phase from all-sky polarimetric images, although further validation and study is warranted. This study was limited to days in which the all-sky polarimeter was running at the same time as our dual-polarization lidar. An expanded study could make use of a more continuously operated all-sky polarimeter [39] and dual-polarization lidar to more completely

explore the potential of this method being applied throughout an annual cycle. Such a study would also benefit from the use of a scanning lidar system to measure the off-zenith cross-polarization ratio. Cloud-base heights along with temperature profiles also can be used to help verify cloud phase. Knobelspiesse et al. showed that a cloud was more polarizing with a smaller cloud optical thickness, full validation of which would require high-quality cloud optical depth retrievals [40,41]. Finally, to more completely compare our results to the simulations presented by Knobelspiesse et al, we would have to use their model and incorporate the environmental conditions and solar and observational geometries from our measured days.

Funding

Air Force Office of Scientific Research (AFOSR) (FA9550-14-1-0140).

Acknowledgments

The views and conclusions contained herein are those of the authors and should not be interpreted as necessarily representing the official policies or endorsements, either expressed or implied, of the Air Force Research Laboratory or the U.S. Government. The authors thank Dr. Kirk Knobelspiesse for helpful discussions.

References

- V. Ramanathan, R. D. Cess, E. F. Harrison, P. Minnis, B. R. Barkstrom, E. Ahmad, and D. Hartmann, "Cloud-Radiative Forcing and Climate: Results from the Earth Radiation Budget Experiment," Science 243(4887), 57–63 (1989).
- O. Boucher, D. Randall, P. Artaxo, C. Bretherton, G. Feingold, P. Forster, V.-M. Kerminen, Y. Kondo, H. Liao, U. Lohmann, P. Rasch, S. K. Satheesh, S. Sherwood, B. Stevens, and X. Y. Zhang, 2013: Clouds and Aerosols. In: Climate Change 2013: The Physical Science Basis. Contribution of Working Group I to the Fifth Assessment Report of the Intergovernmental Panel on Climate Change, (Cambridge University, 2013).
- 3. W. B. Rossow and R. A. Schiffer, "Advances in Understanding Clouds from ISCCP," Bull. Am. Meteorol. Soc. 80(11), 2261–2287 (1999).
- A. Deepak, U. O. Farrukh, and A. Zardecki, "Significance of higher-order multiple scattering for laser beam propagation through hazes, fogs, and clouds," Appl. Opt. 21(3), 439–447 (1982).
- S. Arnon and N. S. Kopeika, "Adaptive optical transmitter and receiver for space communication through thin clouds," Appl. Opt. 36(9), 1987–1993 (1997).
- S. Jaruwatanadilok, A. Ishimaru, and Y. Kuga, "Optical imaging through clouds and fog," IEEE Trans. Geosci. Remote Sens. 41(8), 1834–1843 (2003).
- F. Courvoisier, V. Boutou, J. Kasparian, E. Salmon, G. Mejean, J. Yu, and J. P. Wolf, "Ultraintense light filaments transmitted through clouds," Appl. Phys. Lett. 83(2), 213–215 (2003).
- S. Arnon, D. Sadot, and N. S. Kopeika, "Analysis of optical pulse distortion through clouds for satellite to earth adaptive optical communication," J. Mod. Opt. 41(8), 1591–1605 (1994).
- S. Piazzolla and S. Slobin, "Statistics of link blockage due to cloud cover for free-space optical communications using NCDC surface weather observation data," Proc. SPIE 4635, 138–149 (2002).
- J. R. Key and J. M. Intrieri, "Cloud Particle Phase Determination with the AVHRR," J. Appl. Meteorol. 39(10), 1797–1804 (2000).
- S. Platnick, M. D. King, S. A. Ackerman, W. P. Menzel, B. A. Baum, J. C. Riedi, and R. A. Frey, "The MODIS cloud products: algorithms and examples from Terra," IEEE Trans. Geosci. Remote Sens. 41(2), 459–473 (2003).
- J. C. Chiu, A. Marshak, C. H. Huang, T. Várnai, R. J. Hogan, D. M. Giles, B. N. Holben, E. J. O'Connor, Y. Knyazikhin, and W. J. Wiscombe, "Cloud droplet size and liquid water path retrievals from zenith radiance measurements: examples from the Atmospheric Radiation Measurement Program and the Aerosol Robotic Network," Atmos. Chem. Phys. 12, 10313–10329 (2012).
- K. Sassen, "The Polarization Lidar Technique for Cloud Research: A Review and Current Assessment," Bull. Am. Meteorol. Soc. 72(12), 1848–1866 (1991).
- N. L. Seldomridge, J. A. Shaw, and K. S. Repasky, "Dual-polarization lidar using a liquid crystal variable retarder," OPTICE 45(10), 106202 (2006).
- R. A. Stillwell, R. R. Neely III, J. P. Thayer, M. D. Shupe, and D. D. Turner, "Improved cloud-phase determination of low-level liquid and mixed-phase clouds by enhanced polarimetric lidar," Atmos. Meas. Tech. 11(2), 835–859 (2018).
- A. Lacour, H. Chepfer, M. D. Shupe, N. B. Miller, V. Noel, J. Kay, D. D. Turner, and R. Guzman, "Greenland Clouds Observed in CALIPSO-GOCCP: Comparison with Ground-Based Summit Observations," J. Clim. 30(15), 6065–6083 (2017).

- S. M. Sekelsky and R. E. McIntosh, "Cloud observations with a polarimetric 33 GHz and 95 GHz radar," Meteorol. Atmos. Phys. 59(1-2), 123–140 (1996).
- M. S. Norgren, G. deBoer, and M. D. Shupe, "Observed aerosol suppression of cloud ice in low-level Arctic mixed-phase clouds," Atmos. Chem. Phys. 18(18), 13345–13361 (2018).
- K. I. Strabala, S. A. Ackerman, and W. P. Menzel, "Cloud properties inferred from 8 μm –12-μm data," J. Appl. Meteorol. 33(2), 212–229 (1994).
- J. R. Key and J. M. Intrieri, "Cloud particle phase determination with the AVHRR," J. Appl. Meteorol. 39(10), 1797–1804 (2000).
- D. D. Turner, S. A. Ackerman, B. A. Baum, H. E. Revercomb, and P. Yang, "Cloud Phase Determination Using Ground-Based AERI Observations at SHEBA," J. Appl. Meteorol. 42(6), 701–715 (2003).
- B. A. Baum, P. F. Soulen, K. I. Strabala, M. D. King, S. A. Ackerman, W. P. Menzel, and P. Yang, "Remote sensing of cloud properties using MODIS airborne simulator imagery during SUCCESS. 2. Cloud thermodynamic phase," J. Geophys. Res. 105(D9), 11781–11792 (2000).
- 23. W. H. Knap, P. Stammes, and R. B. A. Koelemeijer, "Cloud thermodynamic-phase determination from near-infrared spectra of reflected sunlight," J. Atmos. Sci. 59(1), 83–96 (2002).
- P. Pilewskie and S. Twomey, "Cloud phase discrimination by reflectance measurements near 1.6 and 2.2 μm," J. Atmos. Sci. 44(22), 3419–3420 (1987).
- P. Pilewskie and S. Twomey, "Discrimination of ice from water in clouds by optical remote sensing," Atmos. Res. 21(2), 113–122 (1987).
- M. J. Tauc, C. L. Baumbauer, B. Moon, L. M. Eshelman, W. Nakagawa, J. A. Shaw, A. M. Abel, and D. W. Riesland, "Cloud thermodynamic phase detection with a 3-channel shortwave infrared polarimeter," Proc. SPIE 10655, 24 (2018).
- J. S. Daniel, S. Solomon, R. W. Portmann, A. O. Langford, C. S. Eubank, E. G. Dutton, and W. Madsen, "Cloud liquid water and ice measurements from spectrally resolved near-infrared observations: A new technique," J. Geophys. Res. 107(D21), 21 (2002).
- K. Knobelspiesse, B. van Diedenhoven, A. Marshak, S. Dunagan, B. Holben, and I. Slutsker, "Cloud thermodynamic phase detection with polarimetrically sensitive passive sky radiometers," Atmos. Meas. Tech. 8(3), 1537–1554 (2015).
- N. J. Pust and J. A. Shaw, "Dual-field imaging polarimeter using liquid crystal variable retarders," Appl. Opt. 45(22), 5470–5478 (2006).
- 30. A. R. Dahlberg, N. J. Pust, and J. A. Shaw, "Effects of surface reflectance on skylight polarization measurements at the Mauna Loa Observatory," Opt. Express 19(17), 16008–16021 (2011).
- N. J. Pust and J. A. Shaw, "Digital all-sky polarization imaging of partly cloudy skies," Appl. Opt. 47(34), H190–H198 (2008).
- N. J. Pust, A. R. Dahlberg, M. J. Thomas, and J. A. Shaw, "Comparison of full-sky polarization and radiance observations to radiative transfer simulations which employ AERONET products," Opt. Express 19(19), 18602– 18613 (2011).
- 33. N. J. Pust and J. A. Shaw, "Wavelength dependence of the degree of polarization in cloud-free skies: simulations of real environments," Opt. Express 20(14), 15559–15568 (2012).
- L. M. Eshelman and J. A. Shaw, "The VIS-SWIR spectrum of skylight polarization," Appl. Opt. 57(27), 7974

 7986 (2018).
- 35. G. Horváth, A. Barta, J. Gál, B. Suhai, and O. Haiman, "Ground-based full-sky imaging polarimetry of rapidly changing skies and its use for polarimetric cloud detection," Appl. Opt. 41(3), 543–559 (2002).
- M. S. Ghonima, B. Urquhart, C. W. Chow, J. E. Shields, A. Cazorla, and J. Kleissl, "A method for cloud detection and opacity classification based on ground based sky imagery," Atmos. Meas. Tech. Discuss. 5(4), 4535–4569 (2012).
- 37. N. A. J. Schutgens, L. G. Tilstra, P. Stammes, and F. M. Breon, "On the relationship between Stokes parameters Q and U of atmospheric ultraviolet/visible/near-infrared radiation," J. Geophys. Res. **109**(D9), D09205 (2004).
- 38. L. M. Eshelman, M. J. Tauc, T. Hashimoto, P. Hooser, K. Gillis, W. Weiss, B. Stanley, G. E. Shaw, and J. A. Shaw, "All-sky polarization measurements of the total solar eclipse on 21 August 2017," Proc. SPIE 10655, Polarization. Measurement, Analysis, and Remote Sensing XIII, 106550L (2018).
- J. A. Shaw, N. J. Pust, B. Staal, J. Johnson, and A. R. Dahlberg, "Continuous outdoor operation of an all-sky polarization imager," Proc. SPIE 7672, 76720A (2010).
- 40. M. D. Shupe, "A ground-based multisensor cloud phase classifier," Geophys. Res. Lett. 34(22), L22809 (2007).
- E. W. Eloranta, High spectral resolution lidar. Lidar: Range-Resolved Optical Remote Sensing of the Atmosphere, (Springer-Verlag, 2005).